ADVANCED MATERIALS

Supporting Information

Liquid-Crystalline Elastomer-Nanoparticle Hybrids with Reversible Switch of Magnetic Memory

Johannes M. Haberl, Antoni Sánchez-Ferrer, Adriana M. Mihut, Hervé Dietsch, Ann M. Hirt, and Raffaele Mezzenga*

Supporting Information for:

Liquid-Crystalline Elastomer-Nanoparticle Hybrids with Reversible Switch of Magnetic Memory

By *Johannes M. Haberl*, and *Antoni Sánchez-Ferrer, Adriana M. Mihut, Hervé Dietsch, Ann M. Hirt, Raffaele Mezzenga**

J. M. Haberl, Dr. A. Sánchez. Ferrer, Prof. R. Mezzenga [*],
ETH Zürich, Department of Health Science and Technology
8092 Zürich, Switzerland
E-mail: raffaele.mezzenga@hest.ethz.ch
Dr. A. M. Mihut[†], Dr. H. Dietsch[††]
Adolphe Merkle Institute and Fribourg Center for Nanomaterials, University of Fribourg
1723 Marly, Switzerland
Prof. A. M. Hirt
ETH Zürich, Department of Earth Science
8092 Zürich, Switzerland

In order to obtain homogeneous liquid-crystalline elastomer nanocomposites with well-dispersed nanoparticles into the network, special care was taken from the early functionalization of the nanoparticles up to their integration in the organic matrix, devoted to prevent sedimentation at any stage of the process. This included sonication and periodic vortexing during the process. More details of the individual steps taken to the synthesis of the hybrid nanocomposites can be summarized as follow:

Synthesis of the liquid-crystalline polymer
Dimethyl biphenyl-4,4-dicarboxylate (12.1 g, 44.8 mmol, 1 eq) was mixed with triethylene glycol (7.06 g, 47.0 mmol, 1.05 eq), and titanium (IV) isopropoxide (5 mg). The mixture was heated to 200 °C in a nitrogen atmosphere for 6 h, and methanol was distilled off. The volatile components were removed and the temperature was increased to 230 °C for 1 h to obtain the liquid-crystalline polymer.[1] In two extra steps, an excess of triethylene glycol (0.025 eq) was added to the mixture repeating the same procedure. The final linear polymer was dissolved in dichloromethane and purified by three times precipitating from methanol to obtain the product as a slightly yellowish glassy material (12.8 g, 70%). ^{1}H NMR (400 MHz, CDCl$_3$) δ = 8.10-7.95 (m, 4H, Ar-H), 7.65-7.50 (m, 4H, Ar-H), 4.50-4.37 (m, 4H, -CO$_2$CH$_2$-), 3.90-3.50 (m, 8.8H, -OCH$_2$-) ppm; MS (MALDI-TOF): M_n = 2920 g·mol^{-1}, M_w = 3510 g·mol^{-1}, *DP* = 7.8, *PDI* = 1.2 (Fig. S1).

Synthesis of the spindle type maghemite nanoparticles (SCH NPs).
In a first step, the bare spindle hematite, α-Fe$_2$O$_3$, nanoparticles (BH NPs) were synthesized based on the method described by Ocaña *et al.*[2] The particles were coated with a layer of silica using the approach of Graf *et al.*[3] based on an initial adsorption of polyvinylpyrrolidone (PVP) on the particles to improve their colloidal stability and the subsequent addition of tetraethylorthosilicate (TEOS) as a precursor for the growth of the silica shell. The silica-coated spindle hematite nanoparticles (SCH NPs) dispersion was dried in an air oven at 90 °C for 24 hours. The dried powder is then annealed in a furnace at 360 °C under a continuous hydrogen gas flow. After 2 hours, the hydrogen flow is turned off and the

powder exposed to air.[4] The furnace temperature is decreased to 240 °C during 2 hours. The obtained maghemite particles (SCM NPs) have a hybrid composition consisting of 70% maghemite and 30% hematite as determined from XRD data with Rietveld method.

Surface functionalization of maghemite nanoparticles
Surface functionalized silica coated maghemite nanoparticles (SCM NPs) were obtained following the previously reported method.[5] The surface modification was ensured using 3-aminopropyltriethoxysilane (APTES) coupling agent (ABCR, Germany) used without previous purification. In a typical example, 1 g of SCM NPs was transferred in a mixture of water (330 mL), absolute ethanol (1 L) and tetramethylammonium (12 mL, 25% solution in methanol). 23.6 g of APTES were added to the mechanically stirred suspension under sonication for 2 h at 20 °C. After stirring the suspension overnight, the obtained amino-functionalized SCM NPs were centrifuged at 10000 rpm for 15 min and redispersed in ethanol, repeating this process five times. Thereafter, the mixture was dispersed in 30 mL of dichloromethane.

Synthesis of the organic-inorganic nanocomposite
A dispersion of MNs in dichloromethane (3.17 g, 2.365 wt-%) was ultrasonicated during 30min, and then added to a triisocyanate crosslinker solution (67.4 mg, 0.130 mmol, 1.0 eq, Basonat HI100-BASF) in freshly distilled dichloromethane (1 mL). The crosslinker and the MNs were kept for 2 h, and the liquid-crystalline polymer (571 mg, 0.391 mmol, 3 eq) was dissolved in dichloromethane (absolute, 1 mL), together with dibutyltin dilaurate (1.55 g, 6 wt-% in dichloromethane). The two mixtures were merged, vortexed, poured in a Petri dish and kept for 18 h. The resulting crosslinked film was heated to 85 °C for 2 days. In order to remove all soluble content swelling in chloroform was used to obtain the final fully crosslinked elastomer (80%).

Methods:
Differential Scanning Calorimetry (DSC) experiments were performed on a DSC 1 calorimeter from Mettler Toledo equipped with a Huber TC100 cooling system, where the nanocomposite was encapsulated in a 40 µL aluminum oxide crucible under nitrogen atmosphere. The sample was analyzed in a temperature range from -20 °C to 200 °C with heating and cooling rates of 10, 15, 20 and 25 K·min^{-1}. The first heating curves were used for removing all thermal history from the sample, and the obtained transition temperatures were extrapolated to the combined 0-heating rate transitions. Bright-field images were taken with a Canon 550D digital camera. Transmission Electron Microscopy (TEM) micrographs were obtained on a Philips CM100-Biotwin microscope operating at 80 kV. The nanocomposite sample was ultramicrotomed using a Diatome diamond knife on a Reichert-Jung UltraCut E Microtome to give 80 nm thick sections. Sections were transferred onto 600-mesh copper grids. For the MNs, the sample was prepared by placing some drops of the 0.1 wt-% silica coated MNs suspension onto a carbon-coated copper grid. Small and Wide Angle X-ray Scattering (SWAXS) experiments were performed using a Rigaku MicroMax-002+ microfocused beam (4 kW, 45 kV, 0.88 mA) with the $\lambda_{Cu\,K\alpha}$ = 0.15418 nm radiation in order to obtain direct information on the scattering patterns. The scattering intensities were collected by a Fujifilm BAS-MS 2025 imaging plate system (15.2 x 15.2 cm^2, 50 µm resolved) and a 2D Triton-200 X-ray detector (20 cm diameter). An effective scattering vector range of 0.05 nm^{-1} < q < 25 nm^{-1} was obtained, where q is the scattering wave vector defined as $q = 4\pi \cdot \sin\theta / \lambda_{Cu\,K\alpha}$ with a scattering angle of 2θ. For the order parameter of the nanoparticles, the SAXS pattern was evaluated at low scattering angles (q = 0.15-0.25 nm^{-1}) that have been related to the nanoparticles orientation previously[6] and where scattering is weak in a neat liquid-crystalline elastomer reference sample (Fig. S7). Low-field magnetic susceptibility

experiments were performed on a Kappabridge MFK1-FA from Agico. High-field magnetic torque experiments were performed with a homebuilt torque magnetometer with an accuracy of $2 \cdot 10^{-3}$ J·kg^{-1}. Detailed information on the instrument and the experimental method were previously published.[7] The ferromagnetic tensors OFF and ON were calculated from 15 measurements, using 6 different magnetic field values from $B = 1000$ mT to 1500 mT (100 mT steps). Uniaxial deformation of the sample at a rate of 1 mm s^{-1} (0.05 s^{-1}) up to $\lambda = 3.2$ lead to a shrinkage in the other two directions according to Poisson's ratio for elastomers. The stretched sample was cut into a piece of length $l'_{z1} = 60$ mm, with a width of $l'_{x1} = 5.1$ mm and a thickness of $l'_{y1} = 0.080$ mm, it was folded two times to $l'_z = 20$ mm and $l'_y = 0.240$ mm (ON). The thin film in the OFF state had a length $l_z = 18.5$ mm width $of\ l_x = 9.1$ mm and thickness of $l_y = 0.140$ mm. At the operating temperature of 80 °C the sample relaxed fast to its original dimensions due to entropic elasticity, as confirmed by X-ray analysis.

Calculation of anisotropic magnetic susceptibility

The calculation of the anisotropy of magnetic susceptibility was done on the basis of a Stoner-Wohlfarth model:[8,9]

As the magnetization M of a sample can be calculated from the volume susceptibility K_v with

$$M = K_v \cdot H \tag{1}$$

at the applied magnetic field H, the anisotropy of magnetic susceptibility

$$K_1/K_2 = M_1/M_2. \tag{2}$$

In order to calculate M in the nanocomposite, we assume that the magnetic properties are the result of an ensemble of non-interacting single-domain particles following the assumptions made by Stoner and Wohlfarth.[8,9] Magnetic coupling of grains or grains and the liquid-crystal[10] is not assessed in this calculation, because of separation and isolation by the silica shell. So the sample magnetization in the measuring direction is proportional to the mean particle magnetization

$$M_{sample,i} \propto \left\langle M_{sample,i} \right\rangle = \frac{\int_0^{\pi/2} P(\theta) \cdot M_i(\theta) \sin\theta d\theta}{\int_0^{\pi/2} P(\theta) \cdot \sin\theta d\theta} \tag{3}$$

with the particle population $P(\theta)$, where θ is the angle between the major particle axis and the applied field H, and i is the measuring direction (parallel to H), z or x. In order to get the orientation distribution function $P(\theta)$ X-ray scattering patterns were evaluated[11,12] in azimuthal steps $a_{m+1/2}$

$$P\left(a_{m+1/2}\right) = \frac{1}{\pi^2} \cdot \frac{N}{\sin a_{m+1/2}} \left[S(m) - S(m+1)\right], \tag{4}$$

where $0 \le m \le (N-1)$,

$$S(m) = \sum_{n=m}^{N-1} I\left(a_{N-n-1/2}\right) \cdot \left[\left(\cos^2 a_m - \cos^2 a_{n+1}\right)^{1/2} - \left(\cos^2 a_m - \cos^2 a_n\right)^{1/2}\right] \tag{5}$$

and

$$a_n = \left(\frac{n}{N}\right) \cdot \frac{\pi}{2}. \tag{6}$$

In order to calculate $M(\theta)$ of individual particles, the magnetic energy U has to be minimized[8]

$$\frac{dU}{d\Phi} = 0, \tag{7}$$

where ϕ is the angle between $M(\theta)$ and the applied field H. The magnetic energy per volume V can be assumed to be the sum of the magnetostatic energy density u_{ms}, due to the demagnetizing field in the shape anisotropic particles, and the Zeeman energy density u_H due to the orientation of these in the magnetic field, when we assume that no magneto-crystalline anisotropy is present.

$$\frac{U}{V} = u_{ms} + u_H \tag{8}$$

with

$$u_{ms} = \left(N_{perpendicular} - N_{parallel}\right) \cdot \frac{M_s^2}{2} \cdot \cos^2(\phi - \theta). \tag{9}$$

If we assume a constant aspect ratio R, which is a reasonable assumption due to the narrow and mono-modal shape distribution that was found for the particles, we can calculate the demagnetizing factors [13]

$$N_{parallel} + 2 \cdot N_{perpendicular} = 1 \tag{10}$$

and

$$N_{parallel} = \frac{1}{R^2 - 1} \cdot \frac{R}{2 \cdot \sqrt{R^2 - 1}} \ln\left(\frac{R + \sqrt{R^2 - 1}}{R - \sqrt{R^2 - 1}}\right). \tag{11}$$

Further, the Zeeman energy density is calculated

$$u_H = M_s \cdot H \cdot \cos\phi. \tag{12}$$

When eq. 9 and eq. 12 are inserted in eq. 8 the differential eq. 7 becomes

$$-\left(N_{perpendicular} - N_{parallel}\right) \cdot M_s^2 \cdot \sin(\phi - \theta)\cos(\phi - \theta) + M_s \cdot H \cdot \sin\phi = 0 \tag{13}$$

or

$$\sin\left[2 \cdot (\phi - \theta)\right] + 2 \cdot h \cdot \sin\phi = 0 \tag{14}$$

with

$$h = \frac{H}{\left[M_s\left(N_{perpendicular} - N_{parallel}\right)\right]}. \tag{15}$$

This equation can be solved numerically following [8]

$$2m\left(1-m^2\right)^{1/2}\cos(2\theta)+\sin(2\theta)\left(1-2m^2\right)\pm 2h\left(1-m^2\right)^{1/2}=0 \tag{16}$$

with $m = M / M_s = \cos\phi$, yielding discrete results for the magnetization

$$M_i(\theta)=M_s \cdot m. \tag{17}$$

For the solution, we chose steps of $\pi / 180$ in the limits of $[0, \pi/2]$. By entering $M_i(\theta)$ as defined by eq. 17, eq. 3 yields $\langle M_{particle,i}\rangle$. From the calculated four energy minima of the magnetization, we chose the maximal magnetization curve (Fig. S5), which should correspond to the global minima of the energy curve; this scenario, which excludes potential intermediate metastable magnetization states, might be one reason for the overestimation of the anisotropic magnetization based on this theoretical calculation.

Thus, eq. 4 had to be solved for the sample when it was measured in z-direction (K_1) and when it was measured in x-direction (K_2). For the OFF state, obviously, the isotropic scattering intensity of the X-ray experiment gave an aspect ratio of $K_1/K_2 = 1$. However, for the ON state, the distribution functions P_1 and P_2 were calculated once peaked around $0°$ and once around $90°$, which were inserted into eq. 2 along with eq. 3. When the measuring field of $H = 200$ A m^{-1}, the aspect ratio of 5.6 and the $M_s = 120$ kA m^{-1} were taken into account $K_1'/K_2' = 2.1$ was obtained.

In figure 3 in the main manuscript, the aspect ratios of the measured susceptibilities are shown as red ellipses for OFF and ON. Inserted, blue ellipses with the aspect ratio of the particles are presented, placed at an angle θ, corresponding to the definition of the 3D order parameter[11, 12]

$$S = \frac{1}{2}\langle 3\cos^2\theta_m - 1\rangle = \frac{\int_0^{\pi/2} P(\theta)\cdot\frac{1}{2}\cdot\left(3\cos^2\theta-1\right)\sin\theta\, d\theta}{\int_0^{\pi/2} P(\theta)\sin\theta\, d\theta}, \tag{18}$$

but in 2D projection. Therefore, the order parameter $S = 0$ corresponds to $\theta_m = 54.7°$ in 3D, which is represented with the ellipse at $\theta = 45°$ in the corresponding 2D projection. In the same manner the order parameter of $S = 0.56$ corresponds to $\theta_m = 32.8°$ in the 3D sample and is shown in its 2D projection at $\theta = 24.5°$.

Supporting figures
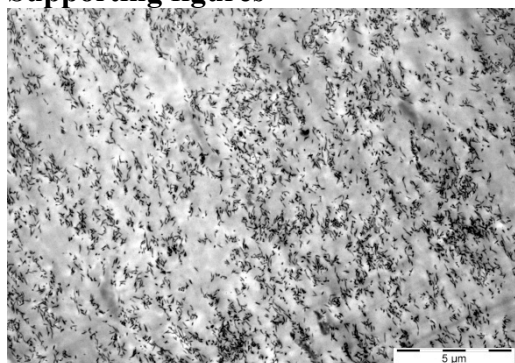
Figure S1 TEM micrographs of the liquid-crystalline elastomer nanocomposite: different regions in the sample all proof the good dispersion with occasional small aggregates of several particles.
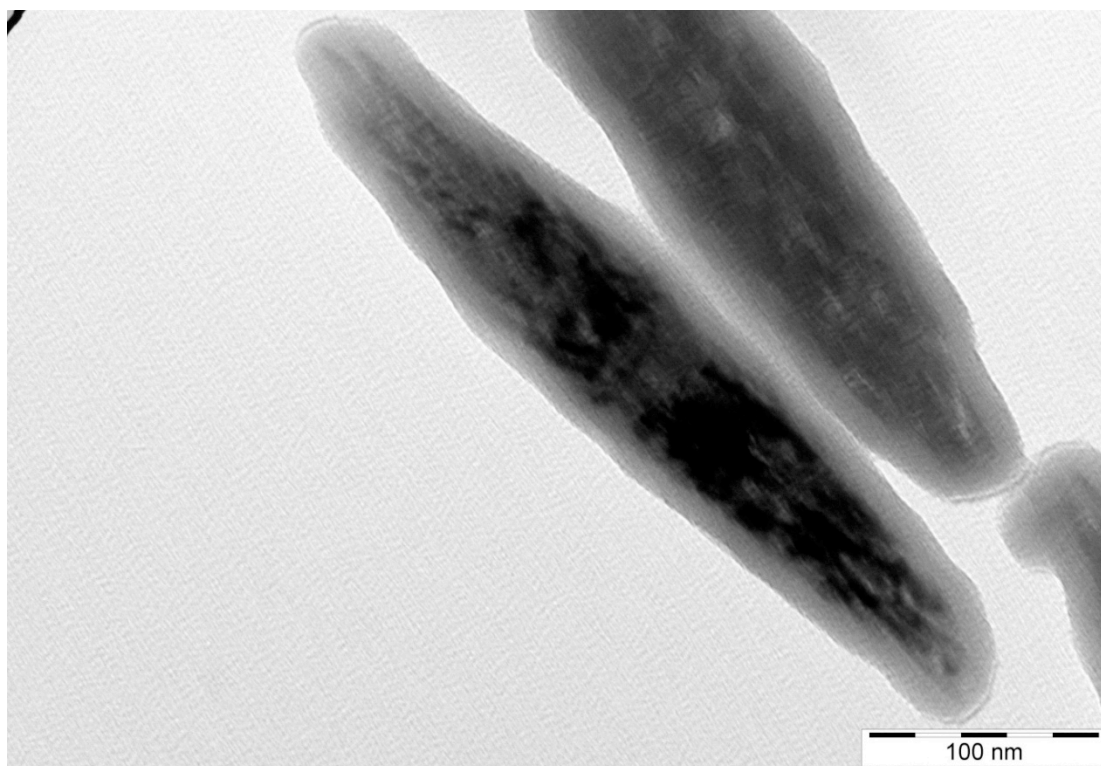

Figure S2 TEM micrographs of the coated maghemite nanoparticles in high resolution: the core-shell-type of the particles is visible. The structure in the darker core region might indicate porosity.
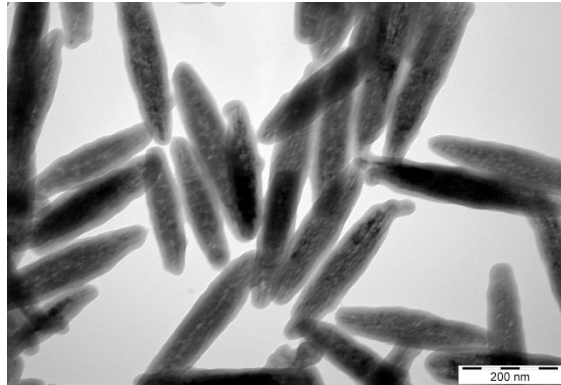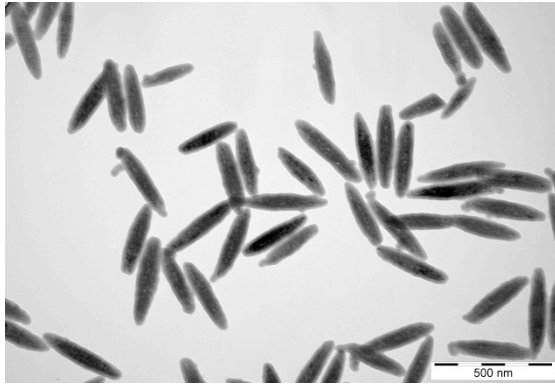
Figure S3 TEM micrographs of the coated maghemite nanoparticles dispersed in water: the aspect ratio of the particles is 5.6 and constant in all particles to a good approximation.
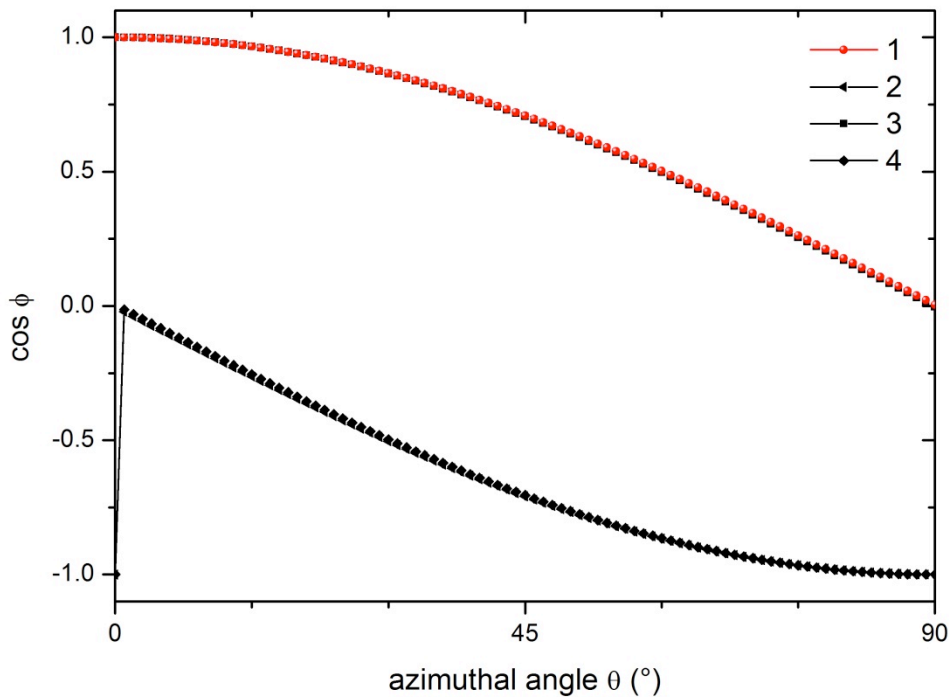

Figure S4 The solutions of the derivative eq. 7 calculated from eq. 16 correspond to the stable (1) and metastable magnetizations (2-4) of the relative magnetization in the measuring direction (proportional to $\cos\phi$) of a particle at the azimuthal angle θ. To proceed further on the calculation, we assumed that all particles would be magnetized at the maximum, e.g. reached the lowest energy configuration, which is indicated with the red curve.
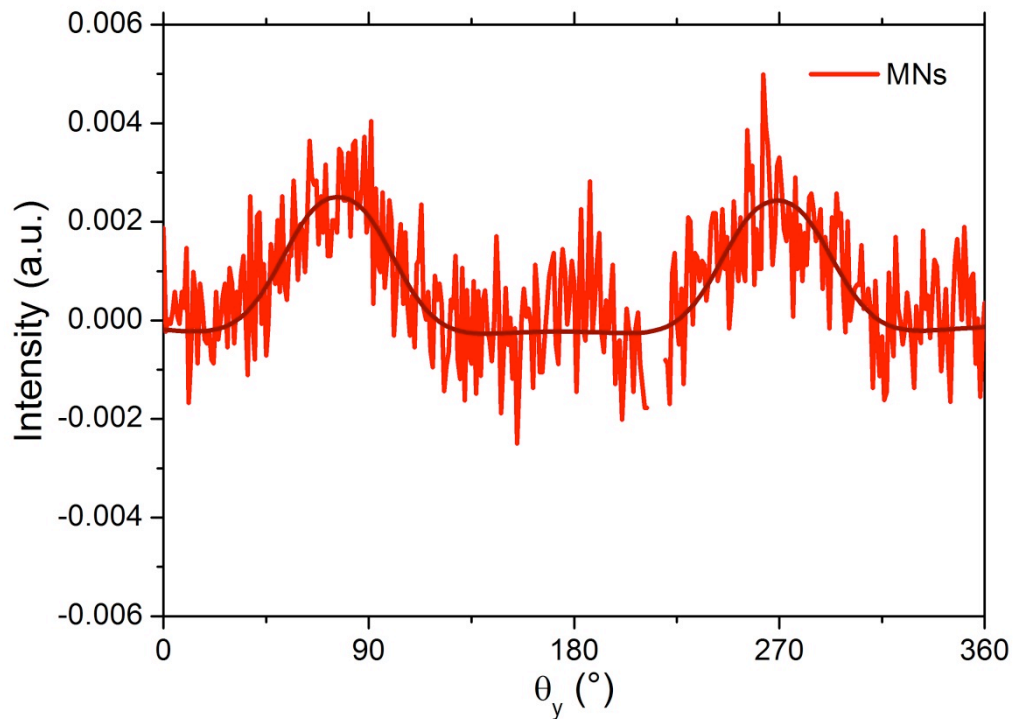
Figure S5 Azimuthal scattering intensity distribution of SAXS experiment performed with the sample ON in *z*-direction. The peaks correspond to the in-layer confined particles after stretching with the degree of order of approximately *S* = -0.04.
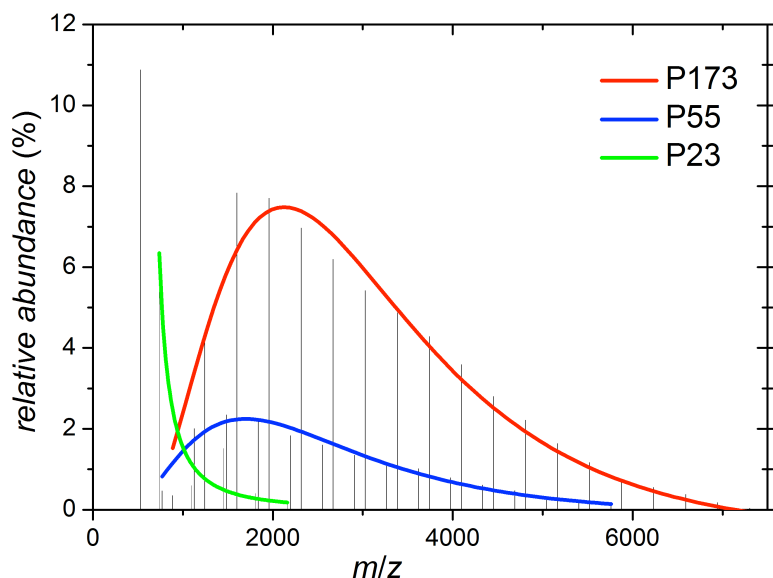
Figure S6 MALDI-TOF mass spectroscopy of the liquid-crystalline polymer in DCTB / Na Mix 1:10:1. 72.2% of the total intensity is assigned to P173 which is the di-hydroxyl terminated chain, 16.5% of the intensity corresponds to P55, the mono-hydroxyl and mono-methyl ester terminated chain that will insert terminal groups in the network, and 9.0% of the intensity corresponds to P23, the macro-cyclic byproduct of the trans-esterification reaction.[14]
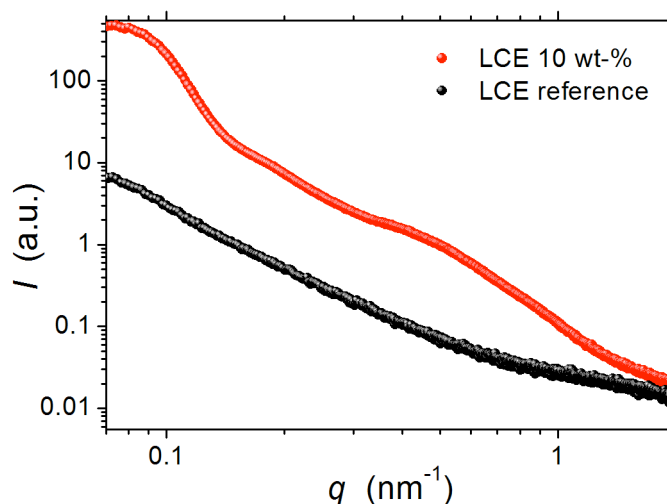
Figure S7 Scattering intensity of the SAXS pattern for the liquid-crystalline elastomer nanocomposite and a neat reference sample.

References

_[1]   A. Martínez-Gómez, E. Pérez, C. Álvarez, *Polymer* **2009,** *50*, 1447-1455.

_[2]   M. Ocaña, M. P. Morales, C. J. Serna, *J. Colloid Interf. Sci.* **1999,** *212*, 317.

_[3]   C. Graf, D. L. J. Vossen, A. Imhof, A. van Blaaderen, *Langmuir* **2003,** *19*, 6693-6700.

_[4]   T. Chappuis, I. Bobowska, S. Hengsberger, E. Vanoli, H. Dietsch, *Chimia* **2011,** *65*, 979-981.

_[5]   A. Sánchez-Ferrer, M. Reufer, R. Mezzenga, P. Schurtenberger, H. Dietsch, *Nanotechnology* **2010,** *21*, 185603.

_[6]   M. Reufer, H. Dietsch, U. Gasser, B. Grobety, A. M. Hirt, V. K. Malik, P. Schurtenberger, *J. Phys.: Condens. Mater.* **2011**, *23*, 065102.

_[7]   F. Bergmüller, C. Bärlocher, B. Geyer, M. Grieder, F. Heller, P. Zweifel, *Meas. Sci. Technol.* **1994**, *5*, 1466-1470.

_[8]   R. C. O`Handley, in *Modern Magnetic Materials: Principles and Applications*, Wiley-Interscience publication, New-York, **1999**.

_[9]   E. C. Stoner, A. Wohlfarth, *E. P. Phil. Trans. R. Soc. A* **1948,** *240*, 599-642.

_[10] D. I. Santiago-Quiñone, A. Acevedo, C. Rinaldi, *J. of Appl. Phys.* **2009**, 105, 07B5121-3.

_[11] G. R. Mitchell, A. Windle, in *Orientation in Liquid Crystal Polymers,* Elsevier Applied Science, London, New York, **1988**.

_[12] R. Lovell, G. R. Mitchell, *Acta. Cryst. A* **1981,** *37*, 135-137.

_[13] J. A. Osborn, *Physical Review* **1945,** *67*, 351-357.

_[14] H. R. Kricheldorf, M. Rabenstein, M. Maskos, M. Schmidt, *Macromolecules* **2001,** *34*, 713-722.